Supplementary Information

Ordering-Induced Concentration Effect: A Mass Transport Boost for CO_2 Electroreduction

Zequn Han[+], Mengqian Li[+], Peipei Li[+], Wenya Fan, Chengbin Zhang, Haohao Duan, Zhijie Wang, Qingxia Chen[*], and Xingchen Jiao[*]

Key Laboratory of Synthetic and Biological Colloids, Ministry of Education, School of Chemical and Material Engineering, Jiangnan University, Wuxi 214122, China.

Email: qxchen@jiangnan.edu.cn; xcjiao@jiangnan.edu.cn

[+]These authors contributed equally to this work.

[*]Corresponding author Email: qxchen@jiangnan.edu.cn; xcjiao@jiangnan.edu.cn

EXPERIMENTAL SECTION

Chemicals:

Silver nitrate ($AgNO_3$, 99.99 %), NaCl, $KHCO_3$, isopropanol, glycerol and DMSO (99.9%) were purchased from Sinopharm Chem. Reagent Co. Ltd. Polyvinyl pyrrolidone (PVP, MW=55000), D_2O and KOH were obtained from Aladdin. The nafion117 was bought from Macklin. Deionized water (18.25 MΩ·cm at 25 ℃, Water Purifier) was used for washing and preparation of solutions. The high purity argon gas (99.9999%) and carbon dioxide (99.999%) were obtained from Wuxi XinXiYi Technology Co., Ltd. The YLS30T carbon paper was purchased from Sinero. All chemicals and materials were used as received without further purification.

Synthesis and purification of Ag NWs:

Ag NWs were synthesized using the polyol method reported previously with modifications[1]. Initially, 5.86 g of PVP and 190 mL of glycerol were added to a 500 mL three-necked flask. The mixture was then heated from room temperature to 110°C within 1 h with gentle stirring at 70 rpm to ensure complete dissolution. Following this, the mixture was allowed to cool naturally to 55°C. 59 mg of NaCl was dissolved in 0.5 mL of H_2O, and this solution was then added to 10 mL of glycerol, followed by thorough stirring. Next, 1.58 g of $AgNO_3$ was added to the PVP solution at 55°C. Once the $AgNO_3$ had fully dissolved, the NaCl solution was added to the mixture, and the temperature was raised to 210°C within 20 min. Upon reaching 210°C, the heating was discontinued, and the mixture was allowed to cool to room temperature naturally. Finally, 200 mL of H_2O was added to the solution at a ratio of 1:1.

The as-synthesized Ag NWs solution was first allowed to stand undisturbed for 12 h. Taking advantage of the distinct sedimentation rates between Ag NWs (characterized by a high aspect ratio and relatively large mass) and Ag nanoparticles (NPs) (featuring small particle sizes and excellent dispersibility), the suspended Ag NPs were partially removed. The supernatant containing minor impurities was carefully decanted, while the Ag NWs-enriched precipitate at the bottom was retained. This sedimentation-decantation cycle was repeated three times to enhance the initial purity of the Ag NWs. Subsequently, the preliminarily purified Ag NWs were dispersed in deionized water containing 0.5wt% PVP, followed by ultrasonication for 10 min to form a homogeneous Ag NWs aqueous dispersion. Acetone was then slowly added to the dispersion at a volume ratio of C_3H_6O:

H_2O = 2.5:1 under gentle stirring. The addition of acetone was ceased when the solution color changed from grayish-green to pale yellow, a phenomenon indicating the initiation of Ag NWs aggregation. Owing to their larger mass, the aggregated Ag NWs rapidly settled to the bottom within 10 min, whereas the supernatant contained unaggregated Ag NPs, short Ag NW fragments, and a small amount of residual PVP. The supernatant was carefully aspirated using a pipette to avoid disturbing the bottom precipitate. Thereafter, deionized water containing 0.5wt% PVP was re-added to the precipitate to reconstitute a homogeneous Ag NWs aqueous dispersion. The acetone addition-sedimentation-supernatant removal process was repeated three times until the supernatant became clear, ultimately yielding a high-purity Ag NWs precipitate. Finally, the Ag NWs precipitate was redispersed in deionized water to obtain a stable colloidal dispersion.

Ordered assembly and transfer of Ag NWs:

Ordered Ag NW array was prepared through the Langmuir-Blodgett (LB) assembly technique[2]. 5 mL of the above dispersion was centrifuged at 8000 rpm for 1 min to collect the solid Ag NWs. Subsequently, 1 mL of DMF was added to ensure even dispersion of Ag NWs. Then, 1 mL of $CHCl_3$ was introduced and mixed thoroughly. The prepared Ag NWs dispersion was slowly dropped onto the water surface in the LB pool until the entire surface was covered. The mixture was allowed to stand for 20 min to facilitate the complete evaporation of $CHCl_3$. Two LB barriers were used to control the spacing of Ag NWs. Compression was halted when the liquid surface formed a metallic Ag mirror and had not yet wrinkled. After standing for another 30 min, a dense and ordered Ag NWs film was obtained. A 1.0 × 1.0 cm strip of gas-diffusion carbon paper was then pre-wetted with water, immersed horizontally ~5 mm below the interface, and allowed to equilibrate for 30 s. Subsequently, the carbon paper was lifted upward slowly while the Ag NW monolayer remained pinned at the air-water boundary. This horizontal lifting protocol ensures intact contact between the NWs and carbon paper without folding or wrinkling. After drying under ambient conditions, the sample was rinsed with Milli-Q water to remove residual surfactant and finally dried under vacuum.

Characterizations:

Transmission electron microscopy (TEM) observations were performed using an HT7800 TEM with an accelerated voltage of 200 KV. Scanning electron microscopy (SEM) images were obtained using the SU8600 SEM. High-resolution TEM (HRTEM) and high-angle annular dark-field scanning transmission electron microscopy (HAADF-STEM) images were captured on Talos

F200X G2 TEM/STEM. X-ray diffraction (XRD) pattern was recorded using the Philips X'Pert Pro Super diffractometer with Cu Kα radiation (λ=1.54178 Å). Small angle x-ray scattering (SAXS) measurement were conducted using the Xeuss 3.0 small angle scattering instrument with a high-intensity microfocal spot fixed copper target light source. The polarized transmission analysis was carried out with a UV-2100PC spectrophotometer. The contact angle was tested using a video optical contact angle measuring instrument of model Theta Flow. Nuclear magnetic resonance (NMR) experiments were performed using a Bruker AVANCE AV III NMR spectrometer operating at 400 MHz. Inductively coupled plasma-mass spectrometry (ICP-MS) was carried out using the Agilent 7850 instrument. X-ray photoelectron spectroscopy (XPS) data were acquired on ESCALAB MKII system with Al Kα (hv=1486.6 eV) as the excitation source. In situ attenuated total reflection surface-enhanced infrared absorption spectroscopy (ATR-SEIRAS) were obtained using a Thermo Scientific Nicolet iS50 spectrometer. In situ Raman spectra were recorded using a HORIBA XploRA PLUS spectrometer.

Electrochemical measurements:

All electrochemical experiments were performed on a VSP-300 Potentiostat workstation (CHI760E C23460d) equipped with a current amplifier (CHI680D C23643). The flow cell device (Chuxi, Shanghai) was used, which consists of two electrolytic chambers separated by an ion exchange membrane (fumasep FAA-3-50) and a gas diffusion chamber, with a working area of 1*1 cm^2. The electrochemical measurement was conducted in a standard three-electrode system. The ordered/disordered Ag NW film was used as the working electrode, the Ag/AgCl electrode was used as the reference electrode, and the nickel foam was used as the counter electrode. During the electrochemical measurement, 1.0 M KOH solution was used as the electrolyte (pH=14) for both the cathode and anode, and the electrolyte flow rate was controlled by a peristaltic pump to 10 mL min^{-1}. The flow rate of CO_2 (99.99%, Wuxi Xinxiyi Technology Co., Ltd.) was set to 30 sccm using a mass flow controller. The electrochemical impedance spectra were recorded over a frequency range from 10^{-1} to 10^5 Hz at a potential of –0.6 V vs. RHE, with an applied amplitude of 5 mV.

The partial current density of CO was calculated as follows[3]:

$$J_{CO} = FE_{CO} \times J_{total}$$

Where J_{CO} is the partial current density of CO, FE_{CO} is the Faraday efficiency of CO, and J_{total} is the total current density.

The CO production rate, R, was calculated using the following equation[4]:

$$R = \frac{I_{total} \times FE_{CO}}{F \times z \times S}$$

Where R is the CO production rate (μmol h^{-1} cm^{-2}), I_{total} is the total current applied during the reaction (A), $FE_{CO}$is the Faradaic efficiency for CO production (%), F is the Faradaic constant (96485 C mol^{-1}), z is the number of electrons transferred per CO molecule formed, which is 2 for the reduction of CO_2 to CO, and S is the geometric surface area of the working electrode (1.0 cm^2).

In the Tafel region of the polarization curve, the relationship between current density and potential can be expressed by the Tafel equation[3]:

$$Tafel\ slope = \frac{\log (J_{CO})}{overpotential}$$

The cathodic energy efficiency (CEE) is the percentage of chemical energy contained in the reduction product to the total input electrical energy, which is calculated as follows[4]:

$$CEE = \frac{E^0_{OER} - E^0_{CO}}{E^0_{OER} - E^0_{applied}} \times FE_{CO} \times 100\%$$

Where CEE is the cathodic energy efficiency, E^0_{OER} is the standard electrode potential for anodic oxygen evolution reaction (1.23 V), and E^0_{CO} is the standard electrode potential for the reduction reaction of the cathode target product CO (–0.1 V). $E^0_{applied}$ is the applied potential and FE_{CO} is the Faraday efficiency of CO.

The conversion of Ag/AgCl reference electrode to RHE was achieved by the following equation[5]:

$$E(V\ vs.RHE) = E(V\ vs.Ag/AgCl) + 0.196V + 0.059 \times pH$$

The Faraday efficiency of gas products was calculated as follows[6]:

$$FE_x(\%) = \frac{Q_x}{Q_{total}} \times 100\% = \frac{z_x \times n \times \varphi_x \times F}{I \times t} \times 100\% = \frac{z_x \times P \times v \times t \times \varphi_x \times F}{I \times t \times R \times T} \times 100\%$$
$$= \frac{z_x \times P \times v \times \varphi_x \times F}{I \times R \times T} \times 100\%$$

Where FE_x is the Faraday efficiency of gas product x, Q_x is the amount of charge required to form gas x, and Q_{total} is the total charge. z_x is the number of electrons transferred during the formation of gas x, n is the total molar content of gas products, φ_x is the volume fraction of gas x determined by gas chromatography, and I is the current (mA). F is Faraday constant (96485 C mol^{-1}), P is the standard atmospheric pressure, R is the gas constant (8.314 J mol^{-1} K^{-1}), T is the temperature (298K), and v is the gas flow rate (30 sccm).

The Faraday efficiency of liquid products was calculated as follows[6]:

$$FE_y(\%) = \frac{Q_y}{Q_{total}} \times 100\% = \frac{z_y \times n_y \times F}{I \times t} \times 100\% = \frac{z_y \times C_y \times V_{liquid} \times F}{I \times t} \times 100\%$$

Where FE_y is the Faraday efficiency of liquid product y, Q_y is the amount of charge required to form the liquid y, and Q_{total} is the total charge. z_y is the number of electrons transferred during the formation of liquid y, n_y is the molar content of liquid y, I is the current (mA), and t is the reaction time (min). C_y is the concentration of liquid y determined by NMR (mol L^{-1}), V_{liquid} is the electrolyte volume (L), and F is Faraday constant (96485 C mol^{-1}).

K^+ adsorption experiment:

The quantity of absorbed K^+ ions was determined by ICP-MS. The sample was immersed in a 0.5 M KOH solution, with the potential maintained at –1.0 V vs RHE. After 2 min of reaction, the sample was transferred into 10 mL of H_2O and gently shaken for 20 s to collect the K^+ ions adsorbed on the electrode surface. This procedure was repeated 10 times to ensure more accurate results.

In situ ATR-SEIRAS experiments:

ATR-SEIRAS spectra were obtained using the Thermo Scientific Nicolet iS50, which was equipped with a liquid nitrogen-cooled MCT detector and a commercial reaction chamber for in-situ high-tech (CIS-ATR-NTP-HEC). An ultra-thin Au coating and a Si crystal with an angle of incidence of 60° were utilized as a reflective element, with Au enhancing the infrared signals and electronic conduction. The electrolyte was a CO_2-saturated 0.5 M $KHCO_3$ solution. The ordered/disordered Ag NW film served as the working electrode, an Ag/AgCl electrode functioned as the reference electrode, and the platinum plate was used as the counter electrode. Chronopotentiometric method was employed for the experiment at various potentials. Based on LSV results, the voltage range was set from 0 to –1.6 V vs. RHE, and the infrared spectra were collected after 15 s of reaction at each voltage.

In situ Raman experiments:

In-situ Raman spectra were collected using the CIS-Raman-EC-U2-H gas diffusion electrochemical cell and HORIBA XploRA PLUS Raman microscopy. The ordered/disordered Ag NW film served as the working electrode, an Ag/AgCl electrode functioned as the reference electrode, the platinum plate was used as the counter electrode, and 1.0 M KOH solution was employed as the electrolyte. Based on LSV results, the voltage range was set from 0 to –1.6 V vs. RHE, with Raman spectra recorded after 15 s of reaction at each voltage. The laser wavelength

employed for these measurements was 532 nm.

COMSOL Multiphysics simulations:

Finite element simulation was performed using COMSOL Multiphysics 6.2[7]. 2D models of ordered and disordered Ag NWs were constructed using 15 Ag NWs. The electric field distribution of the model was simulated and calculated using the Electric Currents (ec) module. The CO_2 distribution of the model was simulated and calculated using the Diluted Substance Transport (tds) physics module. The grid in the model was set to a free triangle grid, the size is intended to be extremely fin. The relative tolerance in the steady-state solver was set to 0.01.

The electric field distribution of the model was simulated and calculated using the current (ec) module with the following formula:

$$E = -\nabla V$$

The dielectric model follows the following formula:

$$D = \varepsilon_0 \varepsilon_r E$$

Where ε_0 and ε_r are the dielectric constant of vacuum and the material, respectively. The conductivity of Ag is 6.3×107 $s\cdot m^{-1}$.

The distribution of CO_2 presents a dynamic equilibrium, following the mass transfer equation and Nernst equation:

$$\nabla J_j + u \cdot \nabla c_j = R_j$$

$$J_j = -D_j \nabla c_j$$

Where J_j is the total flow of matter, R_j is the reaction source of the electrolyte solution, D_j is the diffusion coefficient (D_{CO2} is set to 1.77×10^{-9} m^2 s^{-1}), c_j is the concentration of ions.

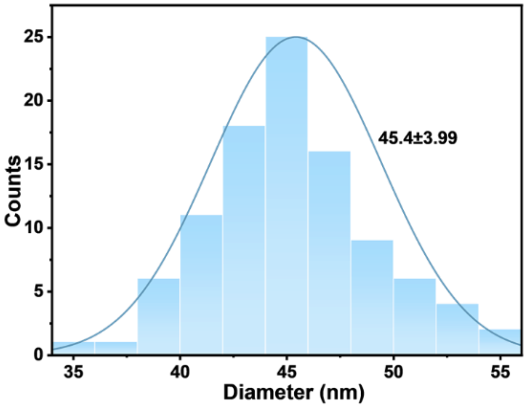

Figure S1. Diameter distribution of Ag NWs.

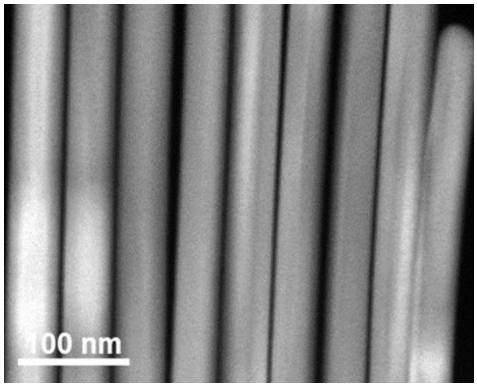

Figure S2. HAADF-STEM image of ordered Ag NWs.

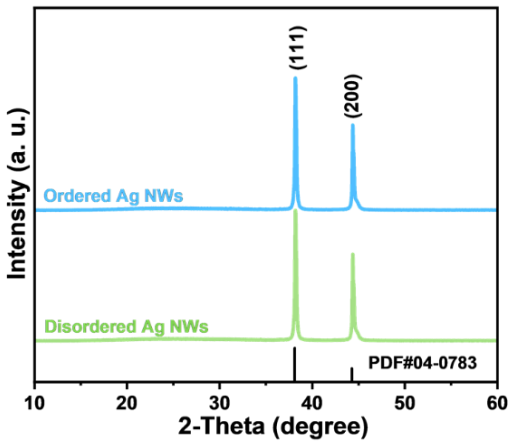

Figure S3. XRD patterns of ordered and disordered Ag NWs.

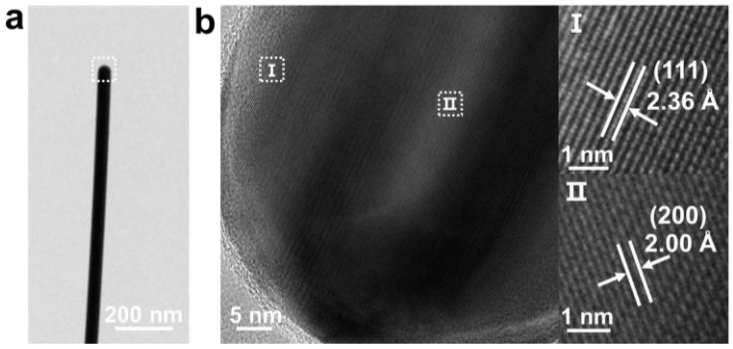

Figure S4. Morphological and structural characterizations of Ag NWs. (a) TEM image. (b) HRTEM images.

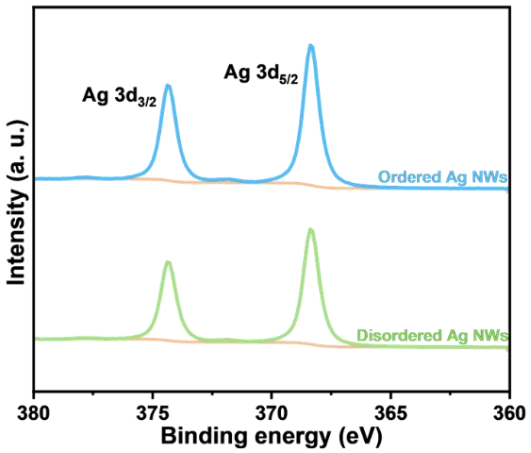

Figure S5. High-resolution XPS spectra of Ag 3d orbital for ordered and disordered Ag NWs.

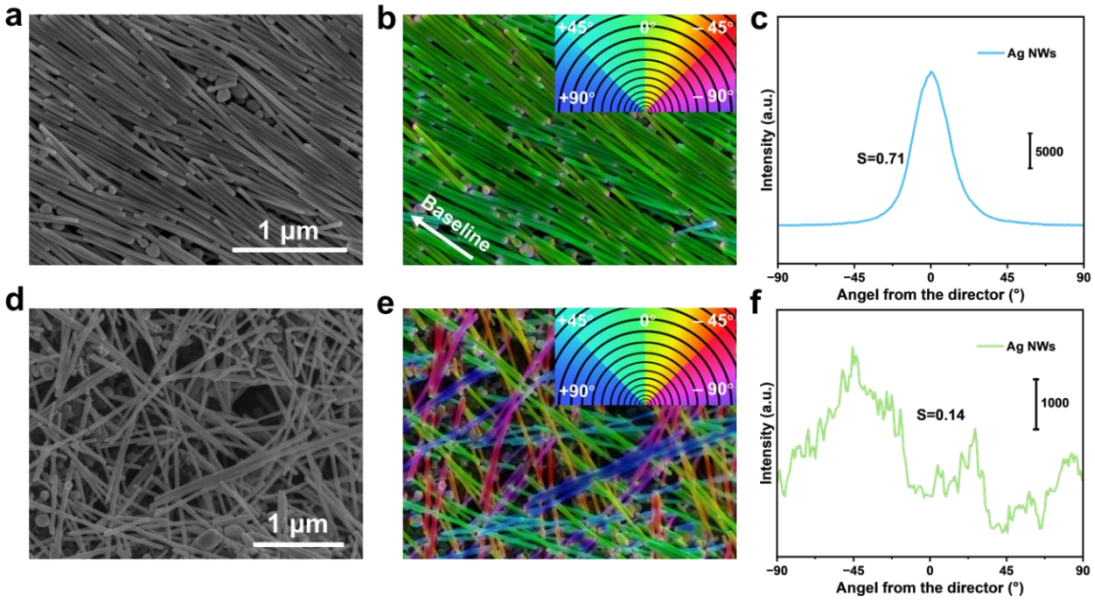

Figure S6. The long-range ordering determination of ordered and disordered Ag NWs. (a) SEM image of ordered Ag NWs. (b) The angular space correlation alignment intensity distributions of ordered Ag NWs. (c) The resulting orientational parameter S of ordered Ag NWs. (d) SEM image of disordered Ag NWs. (e) The angular space correlation alignment intensity distributions of disordered Ag NWs. Insets in b and e: circular color map coding. (f) The resulting orientational parameter S of disordered Ag NWs.

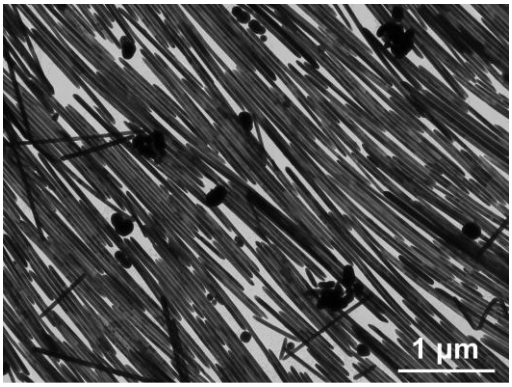

Figure S7. Low-magnification TEM image of ordered Ag NWs.

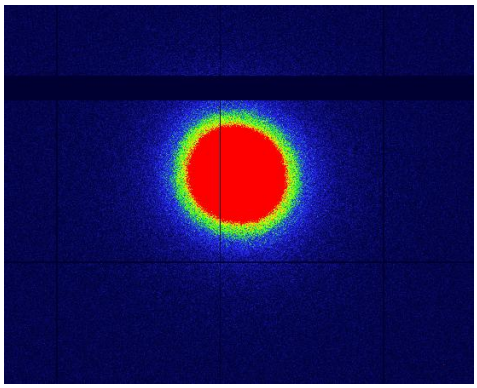

Figure S8. 2D SAXS pattern of disordered Ag NWs.

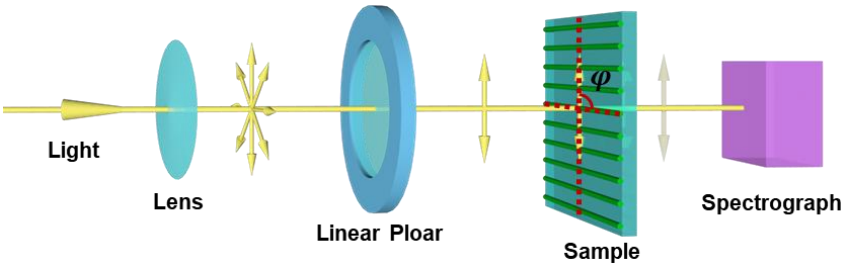

Figure S9. Schematic illustration of the polarized light transmission spectrum measurement.

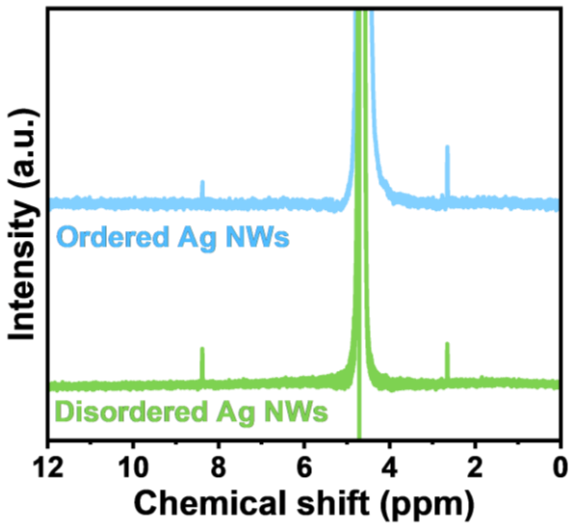

Figure S10. ^{1}H NMR spectra of liquid phase products of ordered and disordered Ag NW catalysts at 100 mA cm^{-2}.

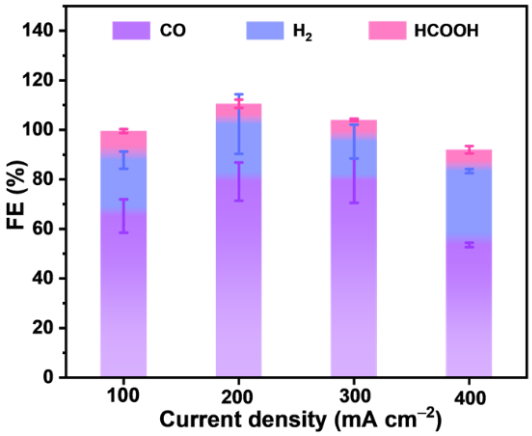

Figure S11. FEs of various products for disordered Ag NWs at different current densities.

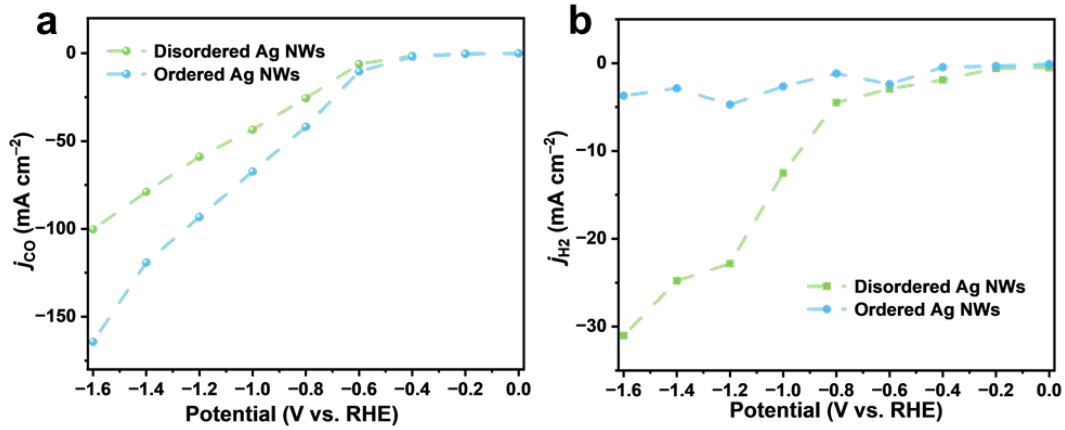

Figure S12. Partial current density of CO and H_2 for ordered and disordered Ag NWs. (a) Partial current density of CO. (b) Partial current density of H_2.

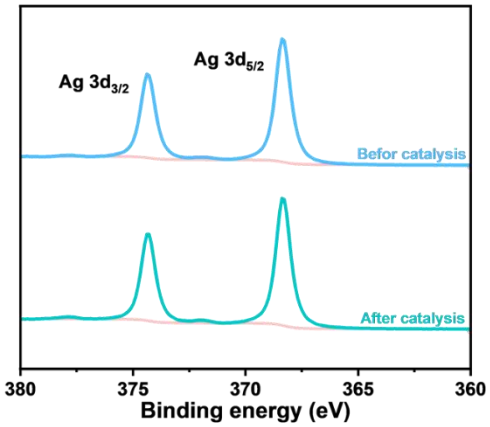

Figure S1. High-resolution XPS spectra of Ag 3d orbital for ordered Ag NWs before and after stability testing.

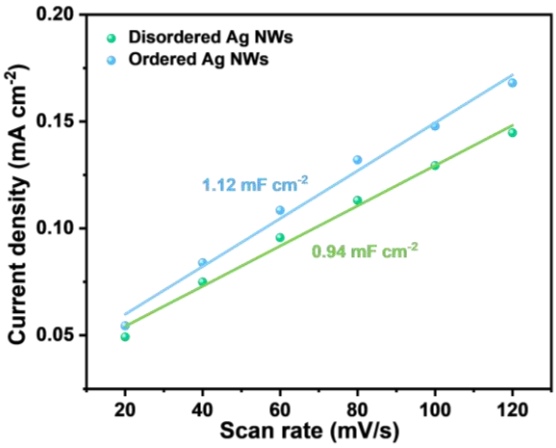

Figure S14. ECSAs of ordered and disordered Ag NWs.

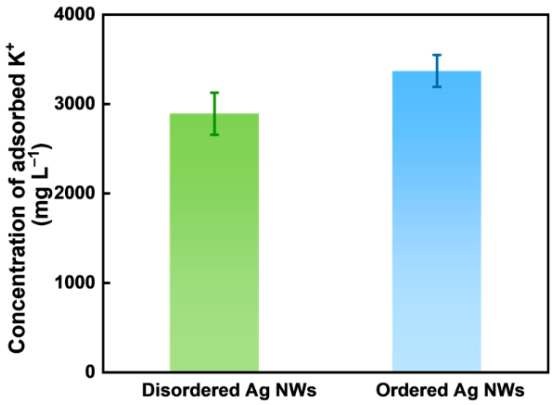

Figure S2. The concentration of adsorbed K^+ induced by the micro electric field in ordered and disordered Ag NWs.

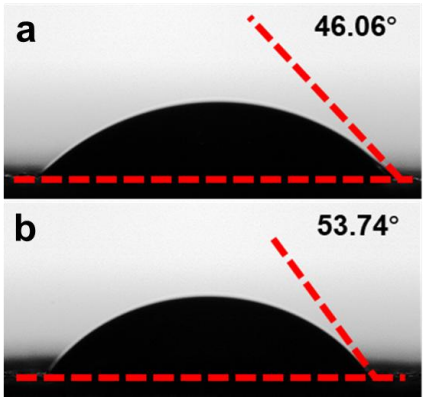

Figure S16. The water contact angles of ordered and disordered Ag NWs. (a) Disordered Ag NWs. (b) Ordered Ag NWs.

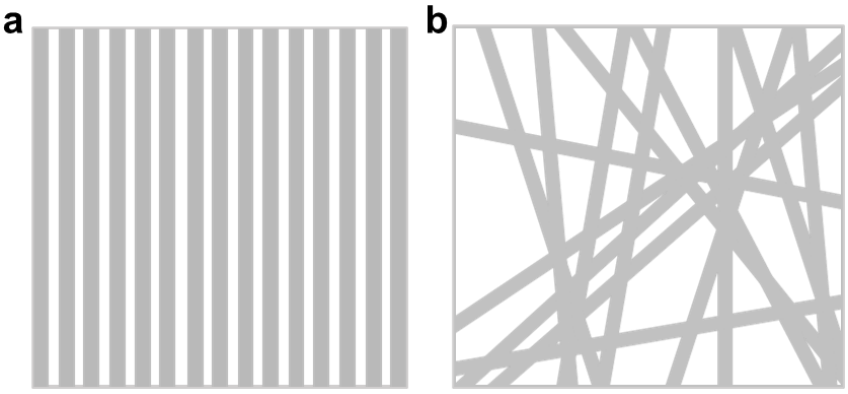

Figure S37. The 2D models of ordered and disordered NWs. (a) Ordered NWs. (b) Disordered NWs.

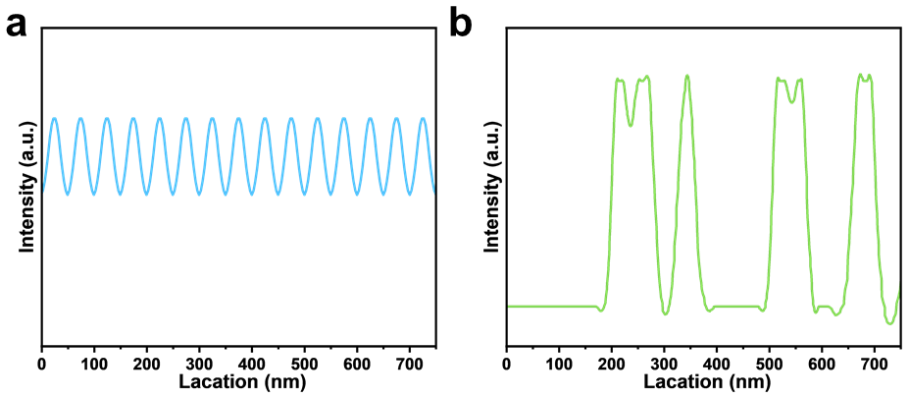

Figure S18. Electric field distribution near the surface of NWs through COMSOL multiple physical simulations. (a) Ordered NWs. (b) Disordered NWs.

References

[1] C. Yang, H. W. Gu, W. Lin, M. M. Yuen, C. P. Wong, M. Y. Xiong, B. Gao, *Adv. Mater.* **2011**, *23*, 3052–3056.

[2] Z. He, J. Su, Y. T. Wang, K. Wang, J. L. Wang, Y. Li, R. Wang, Q. X. Chen, H. J. Jiang, Z. H. Hou, J. W. Liu, S. H. Yu, *J. Am. Chem. Soc.* **2024**, *146*, 19998–20008.

[3] R. Y. Dai, K. A. Sun, R. A. Shen, J. J. Fang, W. C. Cheong, Z. W. Zhuang, Z. B. Zhuang, C. Zhang, C. Chen, *Angew. Chem.Int. Ed.* **2024**, *63*, e202408580.

[4] J. R. Huang, X. F. Qiu, Z. H. Zhao, H. L. Zhu, Y. C. Liu, W. Shi, P. Q. Liao, X. M. Chen, *Angew. Chem.Int. Ed.* **2022**, *61*, e202210985.

[5] A. Dutta, C. E. Morstein, M. Rahaman, A. C. López, P. Broekmann, *ACS Catal.* **2018**, *8*, 8357–8368.

[6] Z. Z. Niu, L. P. Chi, R. Liu, Z. Chen, M. R. Gao, *Energy Environ. Sci.* **2021**, *14*, 4169–4176.

[7] Q. Chen, K. Liu, Y. J. Zhou, X. Q. Wang, K. Z. Wu, H. M. Li, E. Pensa, J. W. Fu, M. Miyauchi, E. Cortés, M. Liu, *Nano Lett.* **2022**, *22*, 6276–6284.